

## Chapter 2

# Control-oriented Models of Braking Dynamics

### 2.1 Introduction

This chapter is devoted to introducing the models of the braking dynamics employed for the design of the different active braking control systems developed in the next chapters, *i.e.*, the single-corner and double-corner models.

As both single-corner and double-corner vehicle models clearly employ a tyre–road friction description, based on which the contact forces can be defined, before introducing the vehicle braking dynamics the force and friction model adopted in this book will be presented.

Note that the treatment of these topics is not intended to provide a comprehensive overview on vehicle modeling nor to present all the available contact forces and tyre–road friction models available in the literature. The aim is to provide the reader with the description of the dynamical models which are of interest for the design of braking control strategies. For a more detailed discussion on these topics, the reader may refer to, *e.g.*, [45, 71, 84].

The chapter is structured as follows. Section 2.2 introduces tyre–road contact forces and presents the adopted friction model. Further, Section 2.3 describes the single-corner model of the braking dynamics, whereas Section 2.4 the double-corner one. In Section 2.5 the considered dynamical models of the braking dynamics are analysed and their linearised version is computed. A numerical analysis of the linearised dynamics is also proposed, to point out the sensitivity of the model dynamics to specific vehicle parameters.

### 2.2 Tyre–road Contact Forces

The tyres are probably the single component that mostly affects the dynamic behaviour and performance of a road vehicle. In fact, the tyre allows contact between the rigid part of the wheel – the hub – and the road surface to take

place on all surfaces and in every road condition. Moreover, the tyre is the means for ensuring adherence to the road and it is responsible for transferring to the ground the vertical load  $F_z$ , which is decomposed – at the contact point on the road plane – into longitudinal  $F_x$  (*i.e.*, traction and braking) and lateral  $F_y$  friction forces, which guarantee the vehicle steerability (see Figure 2.1).

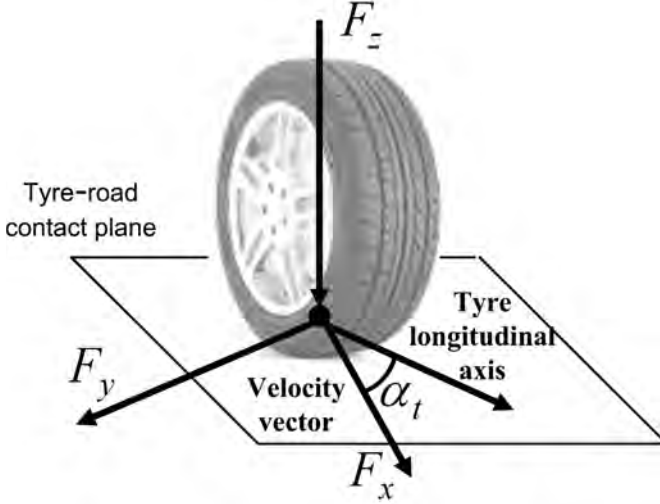


**Figure 2.1** Tyre-road contact forces

Both  $F_x$  and  $F_y$  depend on a large number of features of the road, tyre, and suspensions. Most often, they can be described as

$$F_x = F_x(F_z, \alpha_t, \gamma, \lambda), \quad (2.1)$$

$$F_y = F_y(F_z, \alpha_t, \gamma, \lambda), \quad (2.2)$$

where

- $F_z$  is the vertical force at the tyre-road contact point. In quasi-static conditions it can be simply described as  $F_z = mg$ , where the mass  $m$  can be different for each wheel according to the load distribution of the vehicle and  $g$  represents the gravitational acceleration; in a braking manoeuvre  $F_z$  can significantly change due to dynamic load transfer.
- $\alpha_t$  is the tyre sideslip angle (see Figure 2.1), *i.e.*, the angle between the tyre longitudinal axis and the speed vector of the contact point.
- $\gamma$  is the camber angle, *i.e.*, the tyre inclination with respect to the vertical direction.
- $\lambda$  is the longitudinal wheel slip, *i.e.*, the normalised relative velocity between the road and the tyre, which, in case of zero tyre sideslip angle is

defined as

$$\lambda := \frac{v - \omega r}{\max\{v, \omega r\}}, \quad (2.3)$$

where  $v$  is the wheel ground contact point velocity and  $\omega r$  is the linear speed of the tyre (with radius  $r$  and angular speed  $\omega$ ) at the contact point. The presence of a non-zero slip is due, in general, to traction and braking forces exerted on the tyre. Note that (see also Figure 2.1) a non-zero sideslip angle  $\alpha_t$  modifies the wheel slip expression in (2.3), which takes the form

$$\lambda = \frac{v - \omega r \cos(\alpha_t)}{\max\{v, \omega r \cos(\alpha_t)\}}. \quad (2.4)$$

In the following, we will mostly concentrate on braking manoeuvres (hence  $v \geq \omega r$ ) and consider the assumption of small tyre sideslip angle, *i.e.*, with  $\cos(\alpha_t) \cong 1$ . In this case, (2.3) simply becomes

$$\lambda = \frac{v - \omega r}{v}, \quad (2.5)$$

with  $\lambda \in [0, 1]$ . In particular,  $\lambda = 0$  corresponds to a pure rolling wheel and  $\lambda = 1$  to a locked wheel.

Finally, note that a normalised expression of the vertical forces (2.1) and (2.2) is typically used, which has the form

$$F_x = F_z \mu_x(\alpha_t, \gamma, \lambda), \quad (2.6)$$

$$F_y = F_z \mu_y(\alpha_t, \gamma, \lambda), \quad (2.7)$$

where the proportionality constants  $\mu_x$  and  $\mu_y$ , defined as

$$\mu_x(\alpha_t, \gamma, \lambda) := \frac{F_x}{F_z}, \quad (2.8)$$

$$\mu_y(\alpha_t, \gamma, \lambda) := \frac{F_y}{F_z}, \quad (2.9)$$

are called *longitudinal and lateral friction coefficients*, respectively. It is worth pointing out that the normalised expressions (2.6) and (2.7) rely on the assumption that the relationship between  $F_x$  and  $F_y$  and the vertical load  $F_z$  is linear for all values of  $F_z$ . In fact, this assumption does not rigorously hold for very large values of the vertical load, where the relationship between the forces and the vertical load shows a saturation. However, for control design purposes the simplifying assumption of a linear relationship between  $F_z$  and both  $F_x$  and  $F_y$  can in general be used.

The typical behaviour of the longitudinal and lateral friction coefficients for different values of the tyre sideslip angle  $\alpha_t$  is depicted in Figures 2.2(a) and 2.2(b). These coefficients describe the tyre capability of transferring the vertical load to the ground in longitudinal and lateral direction.

By inspecting Figure 2.2(a) one may notice that all the curves are characterised by a single maximum, and hence exhibit a peak value. Further, note that for  $\lambda = 0$  no longitudinal force can be transmitted to the ground, while for  $\lambda = 1$  (*i.e.*, with locked wheels), there is a loss of longitudinal force up to 20-30% with respect to the peak value. As the tyre sideslip angle  $\alpha_t$  varies, the peak shifts forward in  $\lambda$  as  $\alpha_t$  increases, while the peak value decreases.

On the other hand, from Figure 2.2(b) one may notice that all the curves are monotonically decreasing as functions of  $\lambda$  and they take on their maximum value for  $\lambda = 0$ . Further, note that for  $\lambda = 1$  (*i.e.*, with locked wheels) no lateral force can be transmitted to the ground (independently of the value of  $\alpha_t$ ); hence, with locked wheels there is no residual vehicle steerability. This is one of the main issues that motivate the design of ABS systems. Finally, the lateral friction coefficient increases as the tyre sideslip angle  $\alpha_t$  increases.

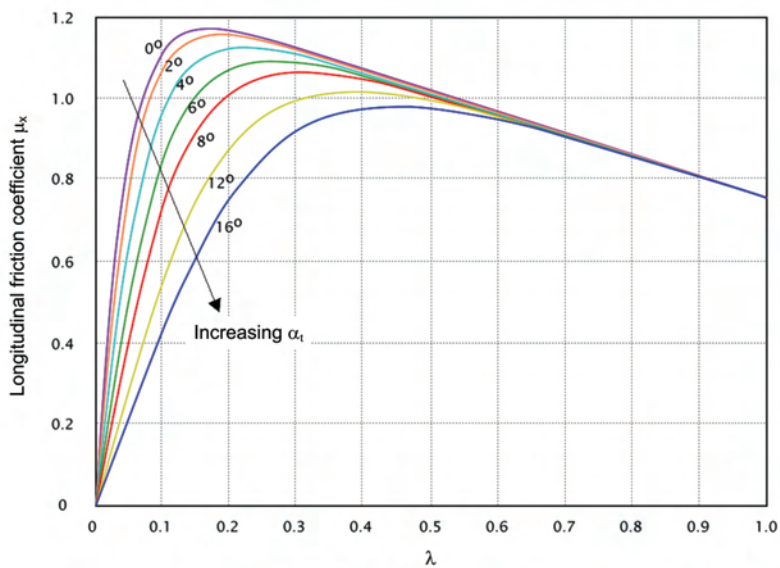
Hence, the behaviour of  $\mu_y$  is somehow dual and complementary with respect to that of  $\mu_x$ , both as a function of  $\lambda$  and of  $\alpha_t$ .

### 2.2.1 Friction Models

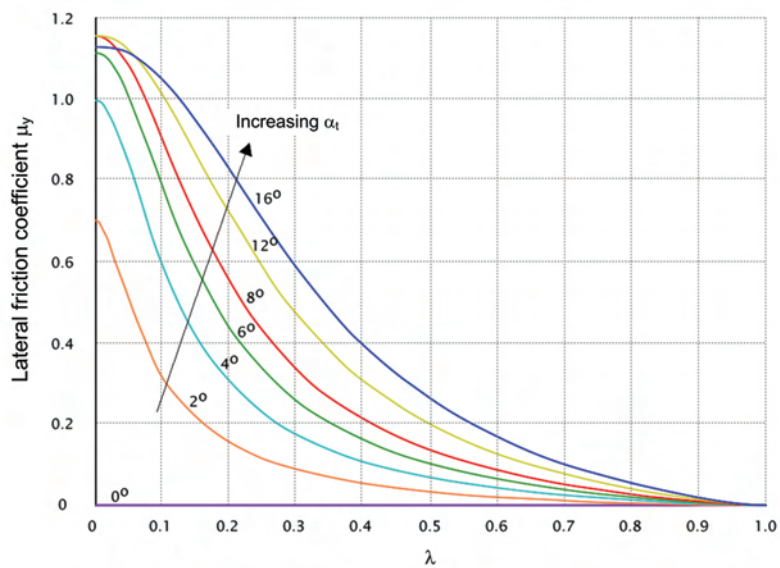
Going back to tyre-road contact forces, one of the most well-known tyre friction models of the form (2.1) and (2.2) is the Pacejka model (see, *e.g.*, [71, 72]), also known as the *magic formula*. The name *magic formula* comes from the fact that the structure of the model equations does not rely on a physical basis and it appears rather complex and with many parameters to be determined. Further, the *magic* comes from the fact that by effectively tuning the parameters such a model does indeed fit a wide variety of tyres in a large range of operating conditions. This model has been shown to suitably match experimental data, obtained under particular steady-state conditions, which assume a constant value of both linear and angular velocities of the tyre. The expression of the longitudinal force in the Pacejka model, under the assumption of symmetric tyres, has the form

$$F_x(F_z, \alpha_t, \gamma, \lambda) = \cos(C_{x\alpha_t} \arctan(B_{x\alpha_t} \alpha_t)) F_{x0}, \quad (2.10)$$

where the expression of the different terms appearing in (2.10) depend on  $F_z$ ,  $\alpha_t$ ,  $\lambda$ ,  $\gamma$  and several constant parameters, which are related to the specific tyre properties and can be identified from experimental data (see, *e.g.*, [71]) according to the following expressions:



(a)



(b)

**Figure 2.2** Plot of the longitudinal (a) and lateral (b) friction coefficient as function of the longitudinal wheel slip  $\lambda$  for different values of the tyre sideslip angle  $\alpha_t$

$$\begin{cases} F_{x0} = D_x \sin[C_x \arctan(B_x \kappa - E_x(B_x \kappa - \arctan(B_x \kappa)))], \\ \kappa = \lambda + H_x, \\ H_x = p_{h1} + p_{h2} df_z, \\ df_z = (F_z - F_{z0})/F_{z0}, \\ D_x = (p_{dx1} + p_{dx2} df_z) F_z, \\ E_x = (p_{ex1} + p_{ex2} df_z + p_{ex3} df_z^2)(1 - p_{ex4} \text{sign}(\kappa)), \\ K_x = F_z(p_{kx1} + p_{kx2} df_z) e^{p_{kx3} df_z}, \\ B_x = K_x / (C_x D_x), \\ B_{x\alpha_t} = (p_{bx1} + p_{dx3} \gamma^2) \cos(\arctan(p_{dx2} \lambda)). \end{cases}$$

The expression of the lateral force  $F_y$ , again under the tyre symmetry assumption, has the form

$$F_y(F_z, \alpha_y, \gamma, \lambda) = \cos(C_y \lambda \arctan(B_y \lambda) F_{x0}), \quad (2.11)$$

where the expression of the different terms appearing in (2.11) depend on  $F_z$ ,  $\alpha_t$ ,  $\lambda$ ,  $\gamma$  and several constant parameters, which are related to the specific tyre properties and can be identified from experimental data according to the following expressions:

$$\begin{cases} F_{y0} = D_y \sin[C_y \arctan(B_y \alpha_y - E_y(B_y \alpha_y - \arctan(B_y \alpha_y))) \\ \quad + C_\gamma \arctan(B_\gamma \gamma - E_\gamma(B_\gamma \gamma - \arctan(B_\gamma \gamma)))], \\ \alpha_y = \alpha_t + H_y, \\ H_y = p_{hy1} + p_{hy2} df_z + (p_{hy3} + p_{hy4} df_z) \gamma, \\ df_z = (F_z - F_{z0})/F_{z0}, \\ D_y = F_z p_{dy1} e^{p_{dy2} df_z} (1 - p_{dy3} \gamma^2), \\ E_y = (p_{ey1} + p_{ey2} df_z)(1 - (p_{ey3} + p_{ey4} \gamma) \text{sign}(\alpha_y)), \\ K_{y\alpha} = p_{ky1} F_{z0} \sin(p_{ky2} \arctan(F_z / ((p_{ky3} + p_{ky4} \gamma^2) F_{z0}))) / (1 + p_{ky5} \gamma^2), \\ B_y = K_{y\alpha} / (C_y D_y), \\ K_{y\gamma} = (p_{ky6} + p_{ky7} df_z) F_z, \\ B_\gamma = K_{y\gamma} / (K_{y\gamma} D_y). \end{cases}$$

The Pacejka friction model is very detailed, and it is the tyre-road friction description most commonly used in commercial vehicle simulators such as, for example, CarSim<sup>®</sup>, Adams/Tire<sup>®</sup>, and Bikesim<sup>®</sup>.

In the rest of the book, for controller design purposes, we will work under the assumptions of small sideslip and camber angles, *i.e.*,  $\alpha_t \cong 0$  and  $\gamma \cong 0$ , and thus consider the longitudinal force only. So, for simplicity, we indicate the friction coefficient  $\mu_x$  with  $\mu$ . Further, we assume a proportionality relationship between normal force and longitudinal force, thus obtaining the longitudinal tyre-road force description

$$F_x = F_z \mu(\lambda). \quad (2.12)$$

This simplification will not affect the design of any of the forthcoming control algorithms. In fact, changes in  $\alpha_t$  and  $\gamma$  cause a shift in the abscissa of the

peak of the the friction coefficient curve  $\mu(\lambda)$  and act as a scaling factor on the curve itself, in this resembling a variation in the vertical load  $F_z$ . Accordingly, as none of the proposed controllers will be designed assuming knowledge of the current value of the vertical load, in the same way they can handle non-zero values of  $\alpha_t$  and  $\gamma$ .

As for the friction model, in this book the Burckhardt model (see, *e.g.*, [16,45]) will be employed, as it is particularly suitable for analytical purposes while retaining a good degree of accuracy in the description of the friction coefficient  $\mu(\lambda)$ . Based on this model, the longitudinal coefficient has the following form:

$$\mu(\lambda; \vartheta_r) = \vartheta_{r1}(1 - e^{-\lambda\vartheta_{r2}}) - \lambda\vartheta_{r3}. \quad (2.13)$$

Notice that the vector  $\vartheta_r$  has three elements only. By changing the values of these three parameters, many different tyre-road friction conditions can be modelled. In Figure 2.3 the shapes of  $\mu(\lambda; \vartheta_r)$  in four different road conditions are displayed. The corresponding parameters values  $\vartheta_r$  are given in Table 2.1.

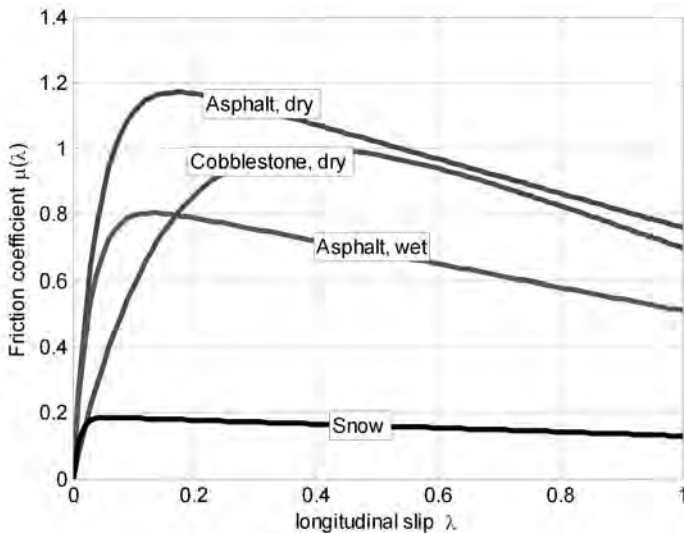


**Figure 2.3** Plot of the function  $\mu(\lambda; \vartheta_r)$  in different road conditions

In the rest of the book these four curves will be used; moreover, the simplified notation  $\mu(\lambda)$  will be adopted, and it will be implicitly assumed that the expression of  $\mu(\lambda)$  may change, according to different road conditions.

Finally, it is worth noting that both the Pacejka and Burckhardt models describe the friction forces *via* static maps, which depend on different parameters. For completeness, we must mention that in the scientific literature dynamic friction models have also been proposed (see, *e.g.*, [127] and the references therein for a complete discussion on this type of friction models).

**Table 2.1** Values of the parameters vector  $\vartheta_r$  for different road conditions

Road condition	$\vartheta_{r1}$	$\vartheta_{r2}$	$\vartheta_{r3}$
Dry asphalt	1.28	23.99	0.52
Wet asphalt	0.86	33.82	0.35
Cobblestone	1.37	6.46	0.67
Snow	0.19	94.13	0.06

### 2.2.2 Relaxation Dynamics

When a rolling pneumatic tyre experiences a step variation in one of the system parameters (*i.e.*, the sideslip angle, the camber angle or the longitudinal wheel slip) both the longitudinal and lateral friction forces undergo a transient leading to a steady-state condition. This mechanism is not an instantaneous phenomenon, mainly due to the time required for the deflection of the tyre. The lag is closely related to the rotation of the tyre, typically taking a fraction of a full revolution of the tyre to effectively reach the steady-state force condition. This distance is often referred to as the *relaxation length*  $s_{0l}$ . Hence, the actual longitudinal and lateral forces  $F_{xAct}$  and  $F_{yAct}$  are computed as

$$\begin{aligned}\dot{F}_{xAct} &= \frac{1}{\tau} (F_x - F_{xAct}), \\ \dot{F}_{yAct} &= \frac{1}{\tau} (F_y - F_{yAct}),\end{aligned}\tag{2.14}$$

where  $F_x$  and  $F_y$  can be computed as in (2.10) and (2.11). The filter time-varying time constant is given by

$$\tau = \frac{s_{0l}}{\omega r},$$

where  $s_{0l}$  is the tyre-relaxation length – usually set equal to half of the tyre circumference – and  $\omega r$  is linear wheel speed at the tyre–road contact point.

From here onward, however, we simply assume that  $F_{xAct} \cong F_x$  and  $F_{yAct} \cong F_y$ , and we refer to the longitudinal and lateral forces with  $F_x$  and  $F_y$ , respectively.

## 2.3 The Single-corner Model

For the preliminary design and testing of braking control algorithms, a simple but effective model known as the *single-corner model* is typically used.

The model is given by the following set of equations (see also Figure 2.4):



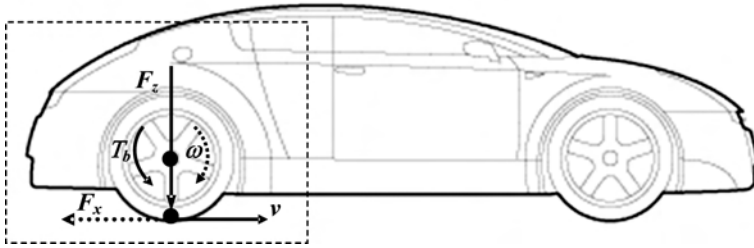


**Figure 2.4** Single-corner model

$$\begin{cases} J\dot{\omega} = rF_x - T_b, \\ m\dot{v} = -F_x, \end{cases} \quad (2.15)$$

where

- $\omega$  [rad/s] is the angular speed of the wheel;
- $v$  [m/s] is the longitudinal speed of the vehicle centre of mass;
- $T_b$  [Nm] is the braking torque;
- $F_x$  [N] is the longitudinal tyre–road contact force; and
- $J$  [kg m<sup>2</sup>],  $m$  [kg] and  $r$  [m] are the moment of inertia of the wheel, the single-corner mass and the wheel radius, respectively.

With reference to Figure 2.4 and system (2.15), the physical meaning of the geometric and vehicle parameters are given in Table 2.2 together with a set of numerical values used in this book for the numerical examples and simulations carried out with the single-corner model.

**Table 2.2** Parameters of the single-corner model

Parameter	Physical meaning	Numerical value
$r$	Wheel radius	0.3 m
$J$	Wheel inertia	1 kg m <sup>2</sup>
$m$	Single-corner mass	225 kg

Throughout the book, the normalised linear wheel deceleration

$$\eta := -\frac{\dot{\omega}r}{g} \quad (2.16)$$

will often be employed. Observe that  $\eta$  is the linear deceleration of the contact point of the tyre, normalised with respect to the gravitational acceleration  $g$ . It is particularly useful since it can be easily compared with the longitudinal deceleration of the vehicle chassis.

Substituting into the first equation of system (2.15) the expression of  $F_x$  given in (2.12) and the definition of the wheel slip in (2.5) yields

$$\begin{cases} J\dot{\omega} = rF_z\mu\left(\frac{v-\omega r}{v}\right) - T_b, \\ m\dot{v} = -F_z\mu\left(\frac{v-\omega r}{v}\right). \end{cases} \quad (2.17)$$

In system (2.17), the state variables are  $v$  and  $\omega$ . As  $\lambda$ ,  $v$  and  $\omega$  are linked by the algebraic relationship (2.5), it is possible to replace the state variable  $\omega$  with the state variable  $\lambda$ .

Specifically, substituting

$$\dot{\lambda} = -\frac{r}{v}\dot{\omega} + \frac{r\omega}{v^2}\dot{v}$$

and

$$\omega = \frac{v}{r}(1 - \lambda)$$

into the first equation of (2.17), one obtains

$$\begin{cases} \dot{\lambda} = -\frac{1}{v} \left( \frac{(1-\lambda)}{m} + \frac{r^2}{J} \right) F_z\mu(\lambda) + \frac{r}{Jv} T_b, \\ m\dot{v} = -F_z\mu(\lambda). \end{cases} \quad (2.18)$$

In the following it is assumed (see, *e.g.*, [41]) that the longitudinal dynamics of the vehicle (expressed by the state variable  $v$ ) are much slower than the rotational dynamics of the wheel (expressed by the state variable  $\lambda$  or  $\omega$ ) due to large differences in inertia. Henceforth,  $v$  can be considered as a slowly-varying parameter. Under this assumption, the second equation (vehicle dynamics) of system (2.15) can be neglected, so that the model reduces to a first-order model of the wheel slip dynamics.

It is worth noticing that the single-corner model relies on the following simplifications:

- The four wheels are treated as *dynamically decoupled*, which means that the dynamic load transfer phenomena induced by pitch motion are neglected. The consequences of this simplification will be subject to a detailed analysis when discussing the double-corner model (see Section 2.4).
- The suspension dynamics are neglected.
- The dependence of the friction forces from the vertical load is modelled as a proportionality relation. This assumption strictly holds only in static conditions. When dynamic load transfer occurs, the dependency is slightly nonlinear with larger directional forces transmitted at lower loads and a saturation effect at very large load values.
- The wheel radius is assumed to be constant. As a matter of fact – during braking – a consequence of the pitch motion is a dynamic change in the wheel radius, which is a function of the instantaneous vertical load.
- Straight-line braking is considered, *i.e.*, the friction forces' dependence on the camber angle  $\gamma$  and on the tyre sideslip angle  $\alpha_t$  is neglected.
- The tyre relaxation dynamics, see Equation 2.14, is not explicitly considered.

Despite these simplifications, the single-corner is the dynamical model most widely employed as a starting point for active braking control systems design (see, *e.g.*, [23, 39–41, 54, 59, 91, 100, 131]) as it provides a simple yet sufficiently rich description of the braking dynamics. Clearly, after having derived a wheel slip control system based on this mathematical model, exhaustive tests should be carried out on a complete vehicle dynamics simulator, so as to verify its performance in a more realistic setting before moving to experimental tests.

As a matter of fact, it is interesting to remark that, despite its simple structure, the design of a feedback controller for (2.18) is far from trivial. In fact, the current road condition and the current value of the vertical load are unknown and can suffer substantial and abrupt changes. Moreover, both the equilibria stability properties and the settling time of the system modes are strongly affected by changes in tyre–road friction characteristics and the normal force exerted on the tyre during braking can experience significant changes due to dynamic load transfer phenomena.

Most of the control approaches presented in this book will be derived from the single-corner model. However, in order to study some important aspects of the braking control systems, such as the interactions between braking control and speed estimation treated in Chapter 5, a more complex model of the vehicle dynamics is needed, capable of describing the link between front and rear axles. Thus, in the next section the double-corner model – which includes load transfer dynamics – is presented.

## 2.4 The Double-corner Model

The *double-corner* model can be regarded as a side view of the vehicle, where one front and one rear wheel are modelled; for our purposes, the main feature of this model is that it allows to describe the load transfer phenomena. It is similar in principle to the *half car* model, which is commonly used to describe the heave dynamics for suspensions control. Consider the double-corner

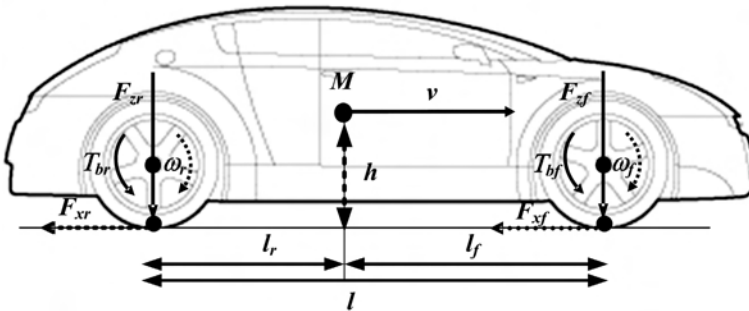


**Figure 2.5** Double-corner model

model shown in Figure 2.5, where the dynamic load transfer is assumed to be proportional to the vehicle deceleration only. Namely, the vehicle dynamics are described by the following set of equations:

$$\begin{cases} J\dot{\omega}_f = r_f F_{x_f} - T_{b_f}, \\ J\dot{\omega}_r = r_r F_{x_r} - T_{b_r}, \\ M\dot{v} = -F_{x_f} - F_{x_r}, \end{cases} \quad (2.19)$$

where

- $\omega_f$  and  $\omega_r$  [rad/s] are the angular speed of the front and rear wheels, respectively.
- $v$  [m/s] is the longitudinal speed of the vehicle centre of mass.
- $T_{b_f}$  and  $T_{b_r}$  [Nm] are the front and rear braking torques, respectively.
- $F_{x_f}$  and  $F_{x_r}$  [N] are the front and rear longitudinal tyre-road contact forces, respectively.
- $J$  [kg m<sup>2</sup>],  $M$  [kg] and  $r_f = r_r = r$  [m] are the moment of inertia of the wheel, the single-corner mass and the wheel radius, respectively (see also Table 2.3). Note that, for simplicity, we assume that the front and rear wheel radii are equal and we denote them both by  $r$ .

For the longitudinal forces  $F_{x_i}$ ,  $i = \{f, r\}$  we use the model in (2.12) and express the tyre-road friction forces *via* the coefficient  $\mu(\lambda)$  given in (2.13). Thus, to complete the model we only have to specify the expression for the vertical load. To describe the load transfer phenomena between front and rear axles, consider the case where the vehicle is subject to a constant acceleration  $\dot{v}$ . In this case, considering the force and torque balance at the projection of the centre of mass to the ground with rotations taken to be positive in clockwise direction, gives

$$\begin{aligned} Mg &= F_{z_f} + F_{z_r}, \\ M\dot{v}h &= -F_{z_f}l_f + F_{z_r}l_r, \end{aligned} \quad (2.20)$$

where (see also Figure 2.5 and Table 2.3)  $l_f$  and  $l_r$  are the distances between the projection of the centre of mass to the ground and the front and rear wheel contact points and  $h$  is the height of the centre of mass from the ground. Solving these equations for  $F_{z_f}$  and  $F_{z_r}$  yields

$$\begin{aligned} F_{z_f} &= W_f - \Delta_{F_z}\dot{v}, \\ F_{z_r} &= W_r + \Delta_{F_z}\dot{v}, \end{aligned} \quad (2.21)$$

where

$$\begin{aligned} W_f &= \frac{Mgl_r}{l}, \\ W_r &= \frac{Mgl_f}{l} \end{aligned} \quad (2.22)$$

are the static vertical loads at the front and rear wheels, and

$$\Delta_{F_z} = \frac{Mh}{l} \quad (2.23)$$

is the coefficient of the load transfer component in (2.21) due to the vehicle acceleration, which is equal and opposite at the front and rear wheels. In (2.22) and (2.23),  $l = l_f + l_r$  is the wheelbase,  $h$  is the height of the centre of mass and  $g$  is the gravitational acceleration.

Note, finally, that  $\dot{v}$  is the vehicle *acceleration*, hence is negative during braking. Thus, Equation 2.21 correctly accounts for the fact that the front wheel experiences a positive load variation in the face of a braking manoeuvre, while the opposite is true for the rear wheel

In system (2.19) the state variables are  $v$  and  $\omega_i$ ,  $i = \{f, r\}$ . As  $\lambda_i$ ,  $v$  and  $\omega_i$  are linked by the algebraic relation (2.5), it is possible to replace  $\omega_i$  with  $\lambda_i$  as state variables in the same way as it was done for the single-corner model. As for the centre of mass longitudinal dynamics in (2.19), based on the description of the longitudinal force in (2.12) and in view of (2.21), it can be re-written as

$$\dot{v} = -\frac{W_f\mu(\lambda_f) + W_r\mu(\lambda_r)}{M - \Delta_{F_z}(\mu(\lambda_f) - \mu(\lambda_r))}. \quad (2.24)$$

To compute the expression of the evolution in time of the front and rear wheel slip  $\lambda_i$ ,  $i = \{f, r\}$ , we consider the longitudinal force description given in (2.12) and the vertical force description (2.21). Further, we compute

$$\dot{\lambda}_i = -\frac{r}{v}\dot{\omega}_i + \frac{r\omega_i}{v^2}\dot{v}$$

and use the relationship

$$\omega_i = \frac{v}{r}(1 - \lambda_i)$$

together with the wheel dynamics in (2.19). This leads to the set of equations

$$\begin{aligned} \dot{\lambda}_f &= -\frac{r}{Jv} (\Psi_f(\lambda_f, \lambda_r) - T_{bf}), \\ \dot{\lambda}_r &= -\frac{r}{Jv} (\Psi_r(\lambda_f, \lambda_r) - T_{br}), \\ \dot{v} &= -\frac{W_f\mu(\lambda_f) + W_r\mu(\lambda_r)}{M - \Delta_{F_z}(\mu(\lambda_f) - \mu(\lambda_r))}, \end{aligned} \quad (2.25)$$

where

$$\Psi_f(\lambda_f, \lambda_r) = \left[ r(W_f - \Delta_{F_z}\dot{v})\mu(\lambda_f) - \frac{J}{r}(1 - \lambda_f)\dot{v} \right], \quad (2.26)$$

$$\Psi_r(\lambda_f, \lambda_r) = \left[ r(W_r + \Delta_{F_z}\dot{v})\mu(\lambda_r) - \frac{J}{r}(1 - \lambda_r)\dot{v} \right]. \quad (2.27)$$

Also in this case, we assume that the longitudinal dynamics of the vehicle are much slower than the rotational dynamics of the wheels due to the differences in inertia. Thus, we regard  $v$  as a slowly-varying parameter and neglect the third equation of model (2.25).

Note that the double-corner model does not include the suspensions dynamics, as the vertical load is modelled *via* the vehicle deceleration only. In the general case, if the dynamics of the suspensions are taken into account and modelled as a linear spring-damper system, the effect on the wheel slip dynamics is the presence of a resonance and an anti-resonance due to the heave and pitch dynamics, usually located at the chassis frequency, which is lower than the frequency range at which wheel dynamics act. As such, the proposed double-corner model is appropriate for braking control systems design in most cases. The analysis of the effects of the neglected dynamics must again be carried out *via* simulations on full vehicle models and finally based on the tests results obtained on the target vehicle. Of course, particular specifications or specific vehicle geometries might require the suspensions dynamics to be considered explicitly in the control-oriented model of the braking dynamics. Such an issue must be evaluated by the control engineer for each specific case.

**Table 2.3** Parameters of the double-corner model

Parameter	Physical meaning	Numerical value
$r$	Front and rear wheel radius	0.3 m
$h$	Height of the centre of mass from ground	0.5 m
$J$	Wheels inertia	1 kg m <sup>2</sup>
$M$	Double-corner mass	450 kg
$l = l_f + l_r$	Wheelbase	2.8 m
$l_f, l_r$	Front and rear axles length	$l_f = 1.2$ m, $l_r = 1.5$ m

## 2.5 Linearised Models and Dynamic Analysis

The first step in the analysis of the braking dynamics is the computation and discussion of the equilibrium points for the considered models, followed by their linearisation around the equilibrium points themselves. Based on the linearised models it will be also possible to carry out a dynamic analysis by means of the study of the system frequency response in order to investigate the model sensitivity to some vehicle parameters of interest.

### 2.5.1 Single-corner Model Analysis

We start by analysing the single-corner model (2.15), computing its equilibrium points and discussing two possible approaches to its linearisation. Further, the transfer function from braking torque to wheel slip will be determined and analysed to illustrate the dynamic dependency of the model on vehicle speed and vertical load.

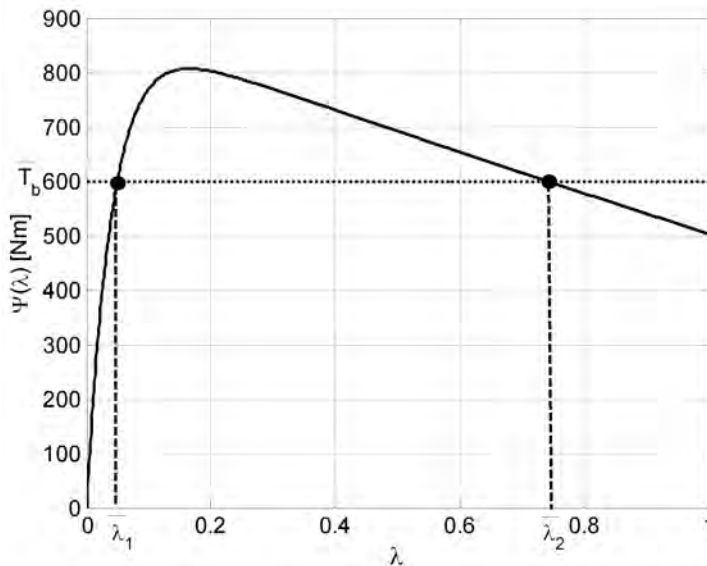


**Figure 2.6** Equilibrium points for the single-corner model (2.29) in the  $(\lambda, T_b)$  plane (example with  $F_z = mg$  and dry asphalt)

#### 2.5.1.1 Equilibrium Points

To compute the equilibrium points note that by setting  $\dot{v} = 0$  and  $\dot{\omega} = 0$  in system (2.15), the corresponding equilibrium is given by  $\lambda = 0$  and  $T_b = 0$ . This corresponds to a constant-speed condition without braking; this equilibrium condition is trivial and meaningless for the design of a braking controller. The equilibrium points we are interested in – during braking – are characterised by  $\dot{\lambda} = 0$ , *i.e.*, constant longitudinal slip  $\lambda = \bar{\lambda}$  and thus constant normalised linear wheel deceleration  $\eta = \bar{\eta}$  (see Equation 2.16). Moreover, note that for any control input  $T_b \geq 0$ , the wheel slip is non-negative, *i.e.*,  $\lambda \geq 0$ . In fact, for non-negative braking torques, the vehicle is either at con-

stant speed or it is braking, and – by the wheel slip definition in (2.5) –  $\lambda \in [0, 1]$  during braking.

According to the assumption of regarding the vehicle speed  $v$  as a slowly-varying parameter, system (2.18) can be formulated as a first-order model of the wheel slip dynamics only in the form

$$\dot{\lambda} = -\frac{1}{v} \left( \frac{(1-\lambda)}{m} + \frac{r^2}{J} \right) F_z \mu(\lambda) + \frac{r}{Jv} T_b, \quad (2.28)$$

which, expressing  $v$  as  $v = \frac{\omega r}{1-\lambda}$  and assuming that  $\lambda \in [0, 1)$ , can be re-written as

$$\dot{\lambda} = -\frac{1-\lambda}{J\omega} (\Psi(\lambda) - T_b), \quad (2.29)$$

with  $\omega > 0$  and

$$\Psi(\lambda) = \left( r + \frac{J}{rm}(1-\lambda) \right) F_z \mu(\lambda). \quad (2.30)$$

When inspecting Equation 2.29, it is obvious that the equilibrium points are characterised by

$$\bar{T}_b = \Psi(\bar{\lambda}). \quad (2.31)$$

Specifically, when  $\mu(\lambda)$  is expressed by means of (2.13) and the control input is constant, *i.e.*,  $T_b = \bar{T}_b$ , the system exhibits the equilibrium points represented, in Figure 2.6, by the intersections between the curve  $\Psi(\lambda)$  and the constant value of the braking torque  $\bar{T}_b$ . To summarise the system behaviour, one may note the following.

1. If  $\bar{T}_b > \max_{\lambda} \Psi(\lambda)$ , the system has no equilibrium points (recall that the model has been derived under the assumption that  $\lambda \in [0, 1)$ ).
2. If  $\bar{T}_b \leq \max_{\lambda} \Psi(\lambda)$ , the system has at most two equilibria, namely  $\bar{\lambda}_1$  and  $\bar{\lambda}_2$  in Figure 2.6, where  $\bar{\lambda}_1 \leq \bar{\lambda}_2$  are the two possibly coincident<sup>1</sup> solutions of

$$\bar{T}_b = \Psi(\lambda). \quad (2.32)$$

As the considered nonlinear system (2.29) is a first-order one, the stability properties of the equilibrium points can be easily investigated by analysing the behaviour of the open-loop vector field in the case  $\bar{T}_b \leq \max_{\lambda} \Psi(\lambda)$ .

To this end, refer to Figure 2.7, where the graph of  $\dot{\lambda}$  as a function of  $\lambda$  is displayed for  $T_b = \bar{T}_b = 600$  Nm, *i.e.*, the same condition depicted in Figure 2.6. As can be seen from the figure (and also by inspecting (2.29))  $\bar{\lambda}_1$  is a locally asymptotically stable equilibrium, while  $\bar{\lambda}_2$  is unstable (see also Appendix A).

Note further that analysing the expression of  $\Psi(\lambda)$  in (2.30), as  $rm \gg J$ , one has  $\Psi(\lambda) \simeq rF_z \mu(\lambda)$ . As such, the wheel slip value corresponding to the

---

<sup>1</sup> Note that the two solutions of (2.32) coincide only if  $\bar{T}_b = \max_{\lambda} \Psi(\lambda)$ .



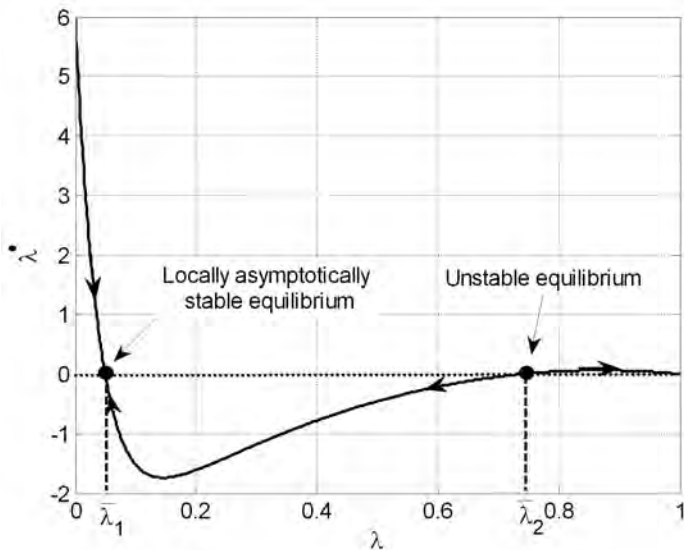


**Figure 2.7** Graph of  $\dot{\lambda}$  as a function of  $\lambda$

abscissa of the maximum of  $\Psi(\lambda)$  is – for all practical purposes – that of the peak of the friction curve.

As such, the nonlinear analysis performed confirms the common knowledge that, for constant values of the braking torque, the equilibria associated with slip values *beyond* the peak of the tyre–road friction curve (see also Figure 2.3) are unstable. It is well known that the optimal trade-off between longitudinal friction force and lateral directional force is achieved if a set-point value for the wheel slip is chosen close to the peak value of the curve  $\mu(\lambda)$ .

A final remark about model (2.29) is due. If we remove the assumption that  $\lambda \in [0, 1)$ , and consider also the value  $\lambda = 1$ , that is completely locked wheels, as an admissible one, then Equation 2.29 clearly shows that  $\lambda = 1$  implies  $\dot{\lambda} = 0$  for all values of the braking torque  $T_b$ , which means that the condition of locked wheels is an equilibrium point for the system. However, as can be seen from Figure 2.7 the point  $\lambda = 1$  is located on the boundary of the domain where the state variable  $\lambda$  is defined and thus its stability properties cannot be directly investigated with the standard analysis tools used in Lyapunov stability theory (see also Appendix A), as the concept of neighbourhood of the equilibrium point cannot be properly defined. Moreover, for model (2.29) to hold one needs  $\omega > 0$ , which in turn implies that  $\lambda$  cannot in fact be equal to 1, but can only approach 1 from the left.

For the design of a braking controller, it is also interesting to express the equilibrium points of the single-corner model in the  $(\lambda, \eta)$  plane. To do this, recall first that the wheel slip definition (2.5) gives

$$\lambda = 1 - \frac{\omega r}{v}, \quad (2.33)$$

which, differentiating with respect to time and letting  $\dot{\lambda} = 0$ , yields

$$\frac{(\omega \dot{v} - v \dot{\omega})}{v^2} = 0,$$

namely

$$\dot{\omega} = \omega \frac{\dot{v}}{v}.$$

By substituting  $\omega = v(1 - \lambda)/r$  and recalling the second equation of system (2.18), one has

$$\dot{\omega} = -\frac{F_z}{mr}(1 - \lambda)\mu(\lambda),$$

which, recalling the definition of  $\eta$  in (2.16), becomes

$$\eta(\lambda) = \Xi(\lambda) := \frac{F_z}{mg}(1 - \lambda)\mu(\lambda), \quad (2.34)$$

which is the desired closed-form expression of the steady-state relationship between  $\eta$  and  $\lambda$ .

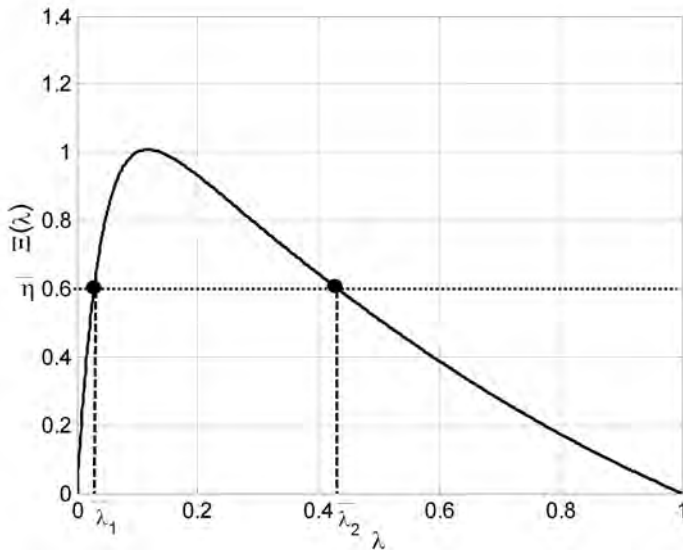


**Figure 2.8** Equilibrium points for the single-corner model (2.29) in the  $(\lambda, \eta)$  plane (example with  $F_z = mg$  and dry asphalt)

In Figure 2.8 the equilibrium manifold  $\Xi(\lambda)$ , see (2.34), is displayed in the  $(\lambda, \eta)$ -domain for case of  $F_z = mg$  and dry asphalt. It is interesting to

observe  $\Xi(\lambda)$  (and thus the normalised wheel deceleration  $\eta$  goes to zero as  $\bar{\lambda}$  approaches 1, *i.e.*, as the wheel locks). Also notice that since  $\Xi(\lambda)$  is a non-monotone function, for each value  $\bar{\eta} \leq \max_{\lambda} \Xi(\lambda)$  there are two admissible slip equilibrium points  $\bar{\lambda}_1$  and  $\bar{\lambda}_2$ , whereas if  $\bar{\eta} > \max_{\lambda} \Xi(\lambda)$  no equilibrium points exist, which is exactly the same condition as that obtained for the case of the braking torque  $T_b$  analysed before for  $\lambda \in [0, 1)$ .

To investigate the stability properties of the equilibrium points, we can carry out the same graphical analysis of the vector field used for the braking torque input, by suitably rearranging the wheel slip dynamic equation and expressing it as a function of the normalised wheel deceleration.

To this end, first note that, substituting the definition of  $\eta$  in the wheel speed dynamics given in the first equation of system (2.17), one obtains that the normalised linear wheel deceleration dynamics are given by

$$\dot{\eta} = \frac{r}{Jg}(T_b - rF_z\mu(\lambda)). \quad (2.35)$$

Substituting this expression together with the equation for the equilibrium manifold  $\Xi(\lambda)$  in (2.34) into the wheel slip dynamics (2.29) and rearranging the equation, one obtains

$$\dot{\lambda} = -g \frac{1 - \lambda}{J\omega} (\Xi(\lambda) - \eta), \quad (2.36)$$

with  $\omega > 0$ .

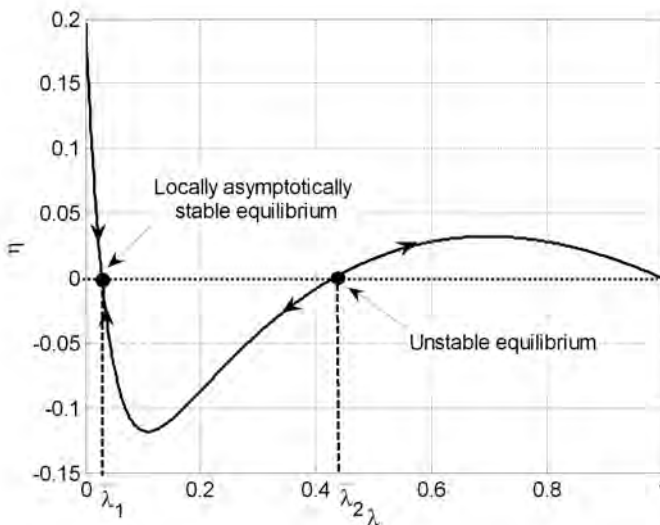


**Figure 2.9** Graph of  $\eta$  as a function of  $\lambda$

The graph of  $\eta$  as a function of  $\lambda$  is shown in Figure 2.9. As can be seen also by inspecting (2.36),  $\bar{\lambda}_1$  is a locally stable equilibrium, while  $\bar{\lambda}_2$  is unstable (see also Appendix A). Note finally that the discussion on the case  $\lambda = 1$  is identical to that carried out previously with reference to the graph of  $\dot{\lambda}$  as a function of  $\lambda$ .

### 2.5.1.2 Model Linearisation

Consider now the following variables, defined around an equilibrium point (characterised by  $\bar{T}_b$ ,  $\bar{\lambda}$ ,  $\bar{\eta}$ ):

$$\delta T_b = T_b - \bar{T}_b; \quad \delta \lambda = \lambda - \bar{\lambda}; \quad \delta \eta = \eta - \bar{\eta}.$$

To carry out the linearisation of the system, a crucial issue is how to consider and manage the dynamic dependency on the variable  $v$ . Often (see, *e.g.*, [41]), a simple quasi-static assumption is made:  $v$  is assumed to be a slowly-varying parameter since it is assumed that the longitudinal dynamics of the vehicle are much slower than the rotational dynamics of the wheel. As such, to linearise the model, the simplest approach is to neglect the second equation (vehicle dynamics) of system (2.15) and work with the first-order model of the wheel dynamics.

To do this, let us define

$$\mu_1(\bar{\lambda}) := \left. \frac{\partial \mu}{\partial \lambda} \right|_{\lambda=\bar{\lambda}}, \quad (2.37)$$

which represents the slope of the  $\mu(\lambda)$  curve around an equilibrium point.

By means of this definition, the friction curve  $\mu(\lambda)$  is replaced by its first-order Taylor series around the equilibrium point  $\bar{\lambda}$ , namely

$$\mu(\lambda) \approx \mu(\bar{\lambda}) + \mu_1(\bar{\lambda})\delta\lambda. \quad (2.38)$$

Linearising the wheel dynamics model (2.28) assuming a constant speed value, *i.e.*,  $v = \bar{v}$ , one obtains

$$\delta \dot{\lambda} = \frac{F_z}{\bar{v}} \left[ \frac{\mu(\bar{\lambda})}{m} - \mu_1(\bar{\lambda}) \left( \frac{(1-\bar{\lambda})}{m} + \frac{r^2}{J} \right) \right] \delta \lambda + \frac{r}{J\bar{v}} \delta T_b.$$

Thus, the transfer function  $G_\lambda(s)$  from  $\delta T_b$  to  $\delta \lambda$  takes the form

$$G_\lambda(s) = \frac{\frac{r}{J\bar{v}}}{s + \frac{F_z}{m\bar{v}} \left[ \mu_1(\bar{\lambda}) \left( (1-\bar{\lambda}) + \frac{mr^2}{J} \right) - \mu(\bar{\lambda}) \right]}. \quad (2.39)$$

Now, linearising the relationship linking  $\eta$  and  $\dot{\omega}$  given in (2.35) one obtains

$$\delta\eta = \frac{r}{Jg}\delta T_b - \frac{r^2}{Jg}\mu_1(\bar{\lambda})F_z\delta\lambda. \quad (2.40)$$

Thus, the transfer function from  $\delta T_b$  to  $\delta\eta$  takes the form

$$G_\eta(s) = \frac{\frac{r}{Jg} \left[ s + \frac{F_z}{m\bar{v}} (\mu_1(\bar{\lambda})(1 - \bar{\lambda}) - \mu(\bar{\lambda})) \right]}{s + \frac{F_z}{m\bar{v}} \left[ \mu_1(\bar{\lambda}) ((1 - \bar{\lambda}) + \frac{mr^2}{J}) - \mu(\bar{\lambda}) \right]}. \quad (2.41)$$

To enlarge the range of validity of the linearised model taking into more direct account the variability of the vehicle speed  $v$ , one may use an intermediate approach: the linearisation is done by explicitly considering the variations of  $v$ , locally around the non-equilibrium value  $\bar{v}$  (namely,  $\delta v = v - \bar{v}$ );  $\bar{v}$  is then considered a slowly-varying parameter in the linearised model.

Thus, no assumptions on the frequency decoupling between chassis and wheel dynamics are while carrying out the linearisation, and the first-order Taylor expansion of the friction curve  $\mu(\lambda)$  becomes

$$\begin{aligned} \mu(\lambda(v, \omega)) &\approx \mu(\bar{\lambda}) + \left[ \frac{\partial \mu}{\partial \lambda} \frac{\partial \lambda}{\partial v} \right] \Big|_{\lambda=\bar{\lambda}} \delta v + \left[ \frac{\partial \mu}{\partial \lambda} \frac{\partial \lambda}{\partial \omega} \right] \Big|_{\lambda=\bar{\lambda}} \delta \omega = \\ &= \mu(\bar{\lambda}) + \mu_1(\bar{\lambda}) \frac{\bar{\omega} r}{\bar{v}^2} \delta v - \mu_1(\bar{\lambda}) \frac{r}{\bar{v}} \delta \omega. \end{aligned} \quad (2.42)$$

Linearising system (2.18) with the above expression for the friction curve one obtains the following second-order linear state space representation

$$\begin{aligned} \dot{x}(t) &= Ax(t) + Bu(t), \\ y(t) &= Cx(t), \end{aligned} \quad (2.43)$$

where  $x = [\delta\omega \quad \delta v]^T$ ,  $u = \delta T_b$  and

$$A = \begin{bmatrix} -\frac{\mu_1(\bar{\lambda})F_z r^2}{J\bar{v}} & \frac{\mu_1(\bar{\lambda})F_z r^2 \bar{\omega}}{J\bar{v}^2} \\ \frac{\mu_1(\bar{\lambda})F_z r}{m\bar{v}} & -\frac{\mu_1(\bar{\lambda})F_z r \bar{\omega}}{m\bar{v}^2} \end{bmatrix}, \quad B = \begin{bmatrix} -\frac{1}{J} \\ 0 \end{bmatrix}.$$

Considering as output the wheel speed  $\delta\omega$ , namely setting  $C = [1 \quad 0]$ , the transfer function from  $\delta T_b$  to  $\delta\omega$  is obtained as

$$G_\omega(s) = C(sI - A)^{-1}B = -\frac{1}{Js} \frac{s + \frac{\mu_1(\bar{\lambda})F_z}{m\bar{v}}(1 - \bar{\lambda})}{s + \frac{\mu_1(\bar{\lambda})F_z}{m\bar{v}}((1 - \bar{\lambda}) + \frac{mr^2}{J})}. \quad (2.44)$$

Note that the pole at the origin of  $G_\omega(s)$  corresponds to the physical situation where, in correspondence to a constant braking torque, the angular wheel speed decreases with constant deceleration.

Recalling now the definition of the normalised wheel deceleration  $\eta$  in (2.16), one obtains

$$G_\eta(s) = -\frac{r}{g}G_{\dot{\omega}}(s) = \frac{r}{Jg} \frac{s + \frac{\mu_1(\bar{\lambda})F_z}{m\bar{v}}(1 - \bar{\lambda})}{s + \frac{\mu_1(\bar{\lambda})F_z}{m\bar{v}} \left( (1 - \bar{\lambda}) + \frac{mr^2}{J} \right)}. \quad (2.45)$$

Finally, *via* Equation 2.40 and Equation 2.45, the transfer function  $G_\lambda(s)$  is obtained as

$$G_\lambda(s) = \frac{r}{J\bar{v}} \frac{1}{s + \frac{\mu_1(\bar{\lambda})F_z}{m\bar{v}} \left( (1 - \bar{\lambda}) + \frac{mr^2}{J} \right)}. \quad (2.46)$$

It is now interesting to compare the transfer functions  $G_\lambda(s)$  and  $G_\eta(s)$  obtained with the two linearisation approaches. The comparison can be carried out considering first the case where  $\mu_1(\bar{\lambda}) \cong 0$ , *i.e.*, when the linearisation point is close to the peak of the friction curve. In this case, the linearised wheel slip dynamics yielded by the first linearisation method, see Equation 2.39, become

$$G_\lambda(s) = \frac{r/J\bar{v}}{s - \frac{F_z}{m\bar{v}}\mu(\bar{\lambda})}, \quad (2.47)$$

while those obtained with the second linearisation method, see Equation 2.46, give

$$G_\lambda(s) = \frac{r/J\bar{v}}{s}. \quad (2.48)$$

As for  $G_\eta(s)$ , the two approaches give the same result due to a zero/pole cancellation<sup>2</sup>, which holds in both cases and yields

$$G_\eta(s) = \frac{r}{Jg}. \quad (2.49)$$

Thus, the first linearisation method yields an unstable linearised system at the peak of the friction curve, while the second one has the peak of the friction curve as stability boundary for the linearised model, which separates the open-loop (locally) asymptotically stable equilibrium points from the unstable ones.

On the other hand, when  $\mu_1(\bar{\lambda})$  is dominant with respect to  $\mu(\bar{\lambda})$  (note that due to the friction curves shape – see Figure 2.3 – this is true for most values of  $\lambda$  on all surfaces except snow), the two linearisation approaches provide comparable results.

In the following, when dealing with the single-corner model we work on the transfer functions obtained with the second linearisation procedure, as it yields models that have the friction curve peak as stability boundary and this better reflects the results obtained with the analysis of the nonlinear model.

Thus, we work with  $G_\lambda(s)$  and  $G_\eta(s)$  having their single pole located at

---

<sup>2</sup> Note that with the first linearisation approach the pole/zero pair which cancels out has positive real part, as the zero and pole have same the expression as the pole of  $G_\lambda(s)$  in (2.47), whereas with the second linearisation approach the cancellation is of a pole/zero pair at the origin (see Equation 2.45).

$$s_p = -\frac{\mu_1(\bar{\lambda})F_z}{m\bar{v}} \left[ (1 - \bar{\lambda}) + \frac{mr^2}{J} \right], \quad (2.50)$$

and with the zero of  $G_\eta(s)$  given by

$$s_z = -\frac{\mu_1(\bar{\lambda})F_z}{m\bar{v}}(1 - \bar{\lambda}). \quad (2.51)$$

### 2.5.1.3 Stability Analysis

Based on the transfer function models (2.46) and (2.45), stability and minimum-phase properties of the linearised system can be analysed easily.

#### Stability Condition Based on $G_\lambda(s)$ and $G_\eta(s)$

The linearised single-corner model with transfer functions  $G_\lambda(s)$  and  $G_\eta(s)$  is asymptotically stable if and only if

$$\frac{\mu_1(\bar{\lambda})F_z}{m\bar{v}} \left[ (1 - \bar{\lambda}) + \frac{mr^2}{J} \right] > 0,$$

which, the term in the brackets being positive, reduces to  $\mu_1(\bar{\lambda}) > 0$ .

This means that  $G_\lambda(s)$  and  $G_\eta(s)$  are open-loop unstable if the equilibrium  $\bar{\lambda}$  occurs beyond the peak of the curve  $\mu(\lambda)$ .

Further, it is worth noting that the transfer function  $G_\eta(s)$  is minimum phase<sup>3</sup> if and only if its pole and zero are in the left half plane and its static gain is positive. The condition on the pole is  $\mu_1(\bar{\lambda}) > 0$ , while the others are given by

$$G_\eta(0) = \frac{g\bar{v}}{\mu_1(\bar{\lambda})F_z} > 0,$$

and

$$\frac{\mu_1(\bar{\lambda})F_z}{m\bar{v}}(1 - \bar{\lambda}) > 0,$$

which can be again reduced to  $\mu_1(\bar{\lambda}) > 0$ .

This means that  $G_\eta(s)$  is non-minimum phase if the equilibrium  $\bar{\lambda}$  occurs beyond the peak of the curve  $\mu(\lambda)$ .

This analysis has shown that the choice of the equilibrium point strongly affects the stability and minimum-phase properties of the linearised single-corner model. Specifically, by applying Lyapunov linearisation method (see Section A.2.1.2), one has that for constant values of the braking torque, the

---

<sup>3</sup> A linear and time-invariant system with transfer function  $G(s)$  is said to be minimum phase if  $G(s)$  has positive gain, all its zeros and poles are in the left half plane and it does not contain any pure delay.

equilibria of system (2.18) associated with slip values beyond the peak of the tyre-road friction curve are unstable, which is consistent with the analysis carried out on the nonlinear system equations.

This instability can hardly be handled by non-professional drivers and it represents another important motivation for the design of ABS systems.

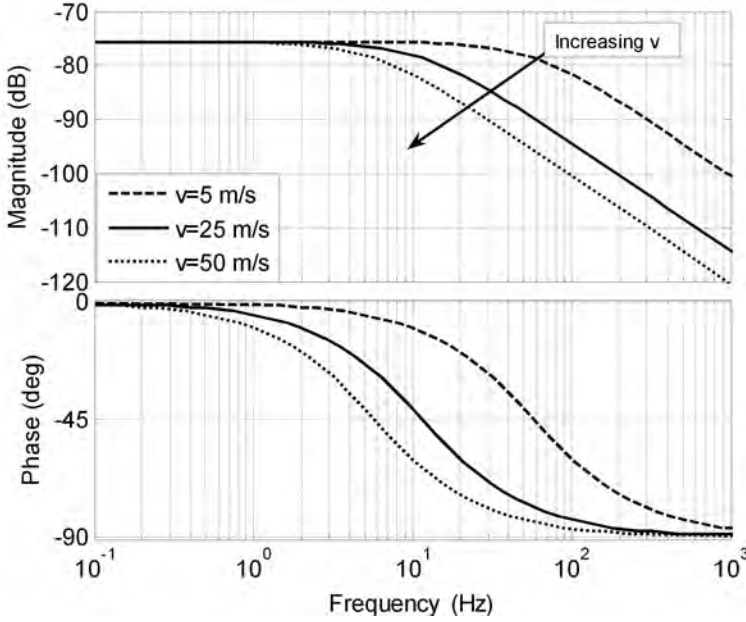


**Figure 2.10** Magnitude and phase Bode plots of the frequency response associated with  $G_\lambda(s)$  for different longitudinal speed values (the nominal linearisation conditions are as in Table 2.4)

### 2.5.1.4 Numerical Sensitivity Analysis

It is now worth analysing the effects that some specific system parameters have on the linearised single-corner dynamics. To this end, we first point out that the nominal linearisation conditions are given in Table 2.4. Based on these, we will now analyse the effect of varying the vehicle speed and the vertical load, the latter being represented by the variable  $F_z$ .

The analysis carried out in the previous section has shown that the longitudinal vehicle speed  $v$ , which is being considered as a slowly-varying parameter, does not affect the stability and minimum-phase properties of the linearised braking dynamics.

However, it has the very awkward effect of acting as a time scale on the wheel dynamics. As a matter of fact, notice that both the pole and the zero



are characterised by the multiplying factor  $1/\bar{v}$ . In Figure 2.10 the magnitude and phase Bode plots of the frequency response associated with  $G_\lambda(s)$  (in the nominal linearisation conditions listed in Table 2.4) are displayed for three different values of  $\bar{v}$ . Note that the angular frequency of the pole of the linearised wheel dynamics for  $v = 3$  m/s is a decade larger than that for  $v = 30$  m/s. Clearly, this scaling effect must somehow be taken into account in the design of a braking controller. This issue was extensively considered in [41], where a simple but effective adaptive control strategy was proposed, using a  $\bar{v}$ -dependent gain-scheduling rationale.

**Table 2.4** Nominal linearisation conditions for the single-corner model

Variable	Steady-state value
$\bar{\lambda}$	0.05
$\bar{T}_b$	600 Nm
$\bar{v}$	25 m/s
$F_z$	mg
Road conditions	Dry asphalt (see Table 2.1)

For braking control design, it is useful to also investigate the effects of the vertical load  $F_z$  on  $G_\lambda(s)$ . To highlight the effect of vertical load variations, it is useful to rewrite  $G_\lambda(s)$  as

$$G_\lambda(s) = \frac{\frac{r}{J\bar{v}}}{s + \left[ \mu_1(\bar{\lambda}) \frac{Ng}{\bar{v}} \left( (1 - \bar{\lambda}) + \frac{mr^2}{J} \right) \right]}, \quad (2.52)$$

where

$$N = \frac{F_z}{mg} \quad (2.53)$$

represents the ratio between the actual vertical load  $F_z$  and its static value  $mg$  and allows us to highlight the effects of the load transfer that occurs during braking.

As can be seen in Figure 2.11, and recalling Figure 2.10, the vertical load mainly affects the low frequency behaviour of  $G_\lambda(s)$ , while the longitudinal speed  $v$  is the dominating effect at high frequency, acting as a scaling on the wheel dynamics. In fact, the static gain of  $G_\lambda(s)$  is given by

$$G_\lambda(0) = \frac{\frac{r}{JN\bar{v}}}{\frac{\mu_1(\bar{\lambda})F_z}{m\bar{v}} \left[ (1 - \bar{\lambda}) + \frac{mr^2}{J} \right]}, \quad (2.54)$$

while the high frequency gain has the form

$$\lim_{s \rightarrow \infty} s G_\lambda(s) = \frac{r}{J\bar{v}}, \quad (2.55)$$

and these expressions explain the behaviour in Figures 2.10 and 2.11.

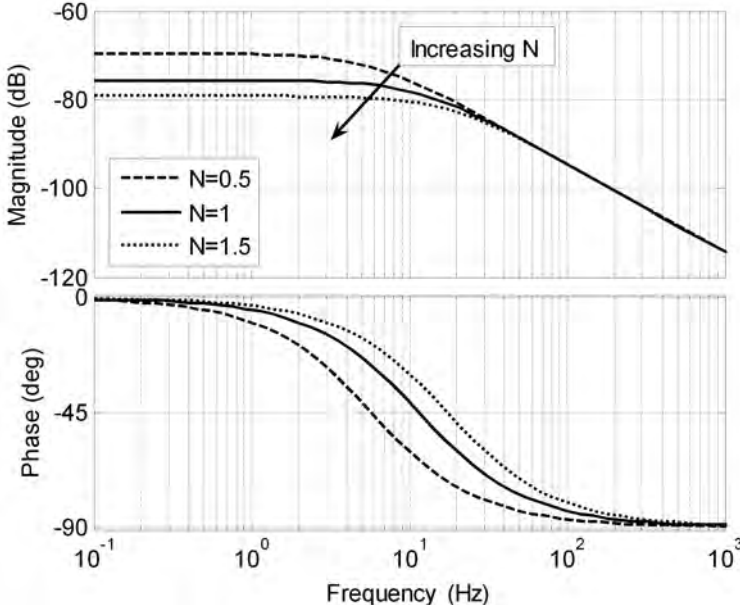


**Figure 2.11** Magnitude and phase Bode plots of the frequency response associated with  $G_\lambda(s)$  for different values of the vertical load (the nominal linearisation conditions are as in Table 2.4)

### 2.5.2 Double-corner Model Analysis

We now analyse the double-corner model introduced in Section 2.4. For this model we will be able to analytically study the system equilibrium points and to carry out the model linearisation explicitly. Further, the transfer function matrix will be obtained. Finally, the proposed dynamical models will be compared based on the analysis of their frequency responses.

#### 2.5.2.1 Equilibrium Points

Once again, we are interested in the equilibrium points characterised by  $\dot{\lambda}_i = 0$ ,  $i = \{f, r\}$ , *i.e.*, constant longitudinal slip  $\lambda_i = \bar{\lambda}_i$ , which in turn yields a constant deceleration  $\dot{v} = \bar{v}$ .

As mentioned in Section 2.4, we work on the first two equations of system (2.25) and consider  $v$  as a parameter. Therefore, the system dynamics we are interested in are given by

$$\begin{cases} \dot{\lambda}_f = -\frac{r}{Jv} (\Psi_f(\lambda_f, \lambda_r) - T_{bf}), \\ \dot{\lambda}_r = -\frac{r}{Jv} (\Psi_r(\lambda_f, \lambda_r) - T_{br}), \end{cases} \quad (2.56)$$

where  $\Psi_f(\lambda_f, \lambda_r)$  and  $\Psi_r(\lambda_f, \lambda_r)$  are as in (2.26) and (2.27), respectively.

Figures 2.12(a) and 2.12(b) show a plot of the functions  $\Psi_f(\cdot, \lambda_r)$  and  $\Psi_r(\lambda_f, \cdot)$ , respectively, obtained for different values of  $\lambda_r$  and  $\lambda_f$ . As it is apparent by inspecting these figures, the front wheel behaviour is substantially independent from that of the rear wheel, while the latter is strongly coupled to the front one.

This can be explained recalling the expression of  $\Psi_f(\cdot, \lambda_r)$  and  $\Psi_r(\lambda_f, \cdot)$  given in (2.26) and (2.27). As a matter of fact, as  $\dot{v}$  is negative during braking,  $\Psi_f(\cdot, \lambda_r)$  and  $\Psi_r(\lambda_f, \cdot)$  are different in magnitude, as the term  $\Delta_{F_z} \dot{v}$  is negative. This difference in magnitude makes  $\Psi_r(\lambda_f, \cdot)$  much more sensitive to the variations in the wheel slip  $\lambda_f$ , which modifies both the numerical value and the shape of the function  $\dot{v}$  in (2.24).

As such, the equilibrium points for each wheel have the form

$$\begin{aligned} \Psi_f(\bar{\lambda}_f, \bar{\lambda}_r) &= \bar{T}_{bf}, \\ \Psi_r(\bar{\lambda}_f, \bar{\lambda}_r) &= \bar{T}_{br}, \end{aligned} \quad (2.57)$$

and thus share the same structure with those analysed for the single-corner model, see Equation 2.31. Thus, the reasoning used in Section 2.5.1 to study the system equilibria for the single-corner model can be applied also in this case. In fact, for both the front and the rear wheels, conditions (2.57) can be pictorially described as in Figure 2.6 and similar conclusions can be drawn.

### 2.5.2.2 Model Linearisation

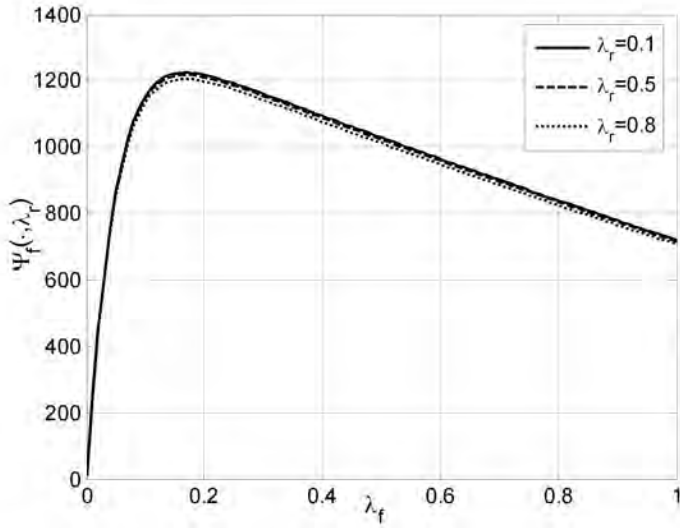
To linearise the double-corner model (2.56), let us define the variables  $\delta\lambda_f = \lambda_f - \bar{\lambda}_f$ ,  $\delta\lambda_r = \lambda_r - \bar{\lambda}_r$ ,  $\delta T_{bf} = T_{bf} - \bar{T}_{bf}$  and  $\delta T_{br} = T_{br} - \bar{T}_{br}$ .

To perform the linearisation we work under the assumption of constant vehicle speed. This choice is motivated by the fact that with this assumption the linearisation procedure can be carried out analytically in a rather simple manner. Of course, the alternative linearisation method considered for the single-corner model in Section 2.5.1 (see in particular Equation 2.42) can be applied also to this case, but the computations are too complex to be analysed explicitly.

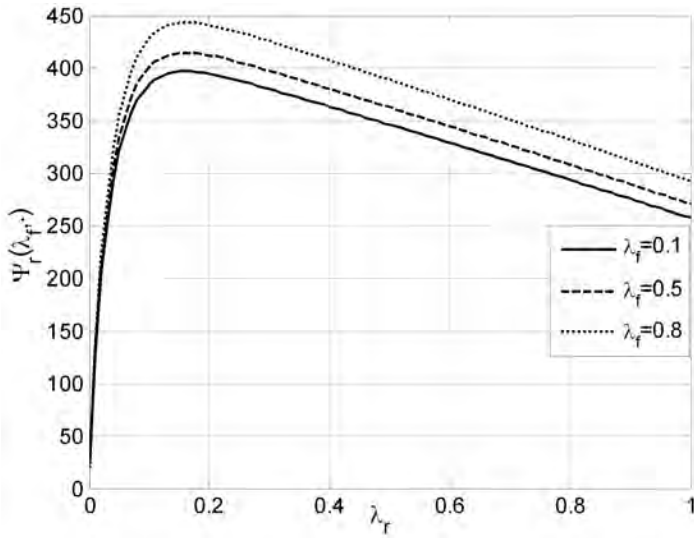
Thus, the Taylor expansion of the tyre-road friction coefficient has the form

$$\mu(\lambda_i) \approx \mu(\bar{\lambda}_i) + \mu_1(\bar{\lambda}_i) \delta\lambda_i, \quad i = \{f, r\}, \quad (2.58)$$

where  $\mu_1(\bar{\lambda})$  is as in (2.37). Further, to simplify the notation of the linearised equations, we introduce the following definition:



(a)



(b)

**Figure 2.12** Plot of (a)  $\Psi_f(\cdot, \lambda_r)$  for different values of  $\lambda_r$ :  $\lambda_r = 0.1$  (solid line),  $\lambda_r = 0.5$  (dashed line) and  $\lambda_r = 0.8$  (dotted line) and (b)  $\Psi_r(\lambda_f, \cdot)$  for different values of  $\lambda_f$ :  $\lambda_f = 0.1$  (solid line),  $\lambda_f = 0.5$  (dashed line) and  $\lambda_f = 0.8$  (dotted line)

$$\delta\bar{\Psi}_{i,j} := \left. \frac{\partial\Psi_i(\lambda_i, \lambda_j)}{\partial\lambda_j} \right|_{\lambda_i=\bar{\lambda}_i, \lambda_j=\bar{\lambda}_j}, \quad i = \{f, r\}. \quad (2.59)$$

Thus, the linearised equations of the double-corner model (2.56) have the form

$$\begin{cases} \delta\dot{\lambda}_f = -\frac{r}{J\bar{v}} (\delta\bar{\Psi}_{f,f}\delta\lambda_f + \delta\bar{\Psi}_{f,r}\delta\lambda_r - \delta T_{b_f}), \\ \delta\dot{\lambda}_r = -\frac{r}{J\bar{v}} (\delta\bar{\Psi}_{r,f}\delta\lambda_f + \delta\bar{\Psi}_{r,r}\delta\lambda_r - \delta T_{b_r}), \end{cases} \quad (2.60)$$

where

$$\begin{aligned} \delta\bar{\Psi}_{f,f} = & rW_f\mu_1(\bar{\lambda}_f) + \left[ r\Delta_{F_z}\mu_1(\bar{\lambda}_f) - \frac{J}{r} \right] \bar{v}_+ \\ & + \left[ r\Delta_{F_z}\mu(\bar{\lambda}_f) + \frac{J}{r}(1 - \bar{\lambda}_f) \right] \bar{v}_{+,f}, \end{aligned} \quad (2.61)$$

$$\delta\bar{\Psi}_{f,r} = \left[ r\Delta_{F_z}\mu(\bar{\lambda}_f) + \frac{J}{r}(1 - \bar{\lambda}_f) \right] \bar{v}_{+,r}, \quad (2.62)$$

$$\delta\bar{\Psi}_{r,f} = \left[ -r\Delta_{F_z}\mu(\bar{\lambda}_r) + \frac{J}{r}(1 - \bar{\lambda}_r) \right] \bar{v}_{+,f}, \quad (2.63)$$

$$\begin{aligned} \delta\bar{\Psi}_{r,r} = & rW_r\mu_1(\bar{\lambda}_r) - \left[ r\Delta_{F_z}\mu_1(\bar{\lambda}_r) + \frac{J}{r} \right] \bar{v}_+ \\ & - \left[ r\Delta_{F_z}\mu(\bar{\lambda}_r) - \frac{J}{r}(1 - \bar{\lambda}_r) \right] \bar{v}_{+,r}, \end{aligned} \quad (2.64)$$

and

$$\bar{v}_+ = \frac{W_f\mu(\bar{\lambda}_f) + W_r\mu(\bar{\lambda}_r)}{M - \Delta_{F_z}[\mu(\bar{\lambda}_f) - \mu(\bar{\lambda}_r)]}, \quad (2.65)$$

$$\bar{v}_{+,f} = \frac{W_f\mu_1(\bar{\lambda}_f)}{M - \Delta_{F_z}[\mu(\bar{\lambda}_f) - \mu(\bar{\lambda}_r)]} + \Delta_{F_z}\mu_1(\bar{\lambda}_f) \frac{W_f\mu(\bar{\lambda}_f) + W_r\mu(\bar{\lambda}_r)}{(M - \Delta_{F_z}[\mu(\bar{\lambda}_f) - \mu(\bar{\lambda}_r)])^2}, \quad (2.66)$$

$$\bar{v}_{+,r} = \frac{W_r\mu_1(\bar{\lambda}_r)}{M - \Delta_{F_z}[\mu(\bar{\lambda}_f) - \mu(\bar{\lambda}_r)]} - \Delta_{F_z}\mu_1(\bar{\lambda}_r) \frac{W_f\mu(\bar{\lambda}_f) + W_r\mu(\bar{\lambda}_r)}{(M - \Delta_{F_z}[\mu(\bar{\lambda}_f) - \mu(\bar{\lambda}_r)])^2}. \quad (2.67)$$

The expressions obtained are useful for deriving the transfer function matrix

$$G(s) = \begin{bmatrix} \delta\lambda_f \\ \delta\lambda_r \end{bmatrix} = \begin{bmatrix} G_{ff}(s) & G_{fr}(s) \\ G_{rf}(s) & G_{rr}(s) \end{bmatrix} \begin{bmatrix} \delta T_{bf} \\ \delta T_{br} \end{bmatrix}, \quad (2.68)$$

which describes the wheel slip dynamics of the double-corner model.

To compute the expression of the transfer function matrix in (2.68), consider that system (2.60) has the following second-order state space representation:

$$\begin{aligned} \dot{x}(t) &= Ax(t) + Bu(t), \\ y(t) &= Cx(t), \end{aligned} \quad (2.69)$$

where  $x = [\delta\lambda_f \ \delta\lambda_r]^T$  and  $u = [\delta T_{bf} \ \delta T_{br}]^T$ , and

$$\begin{aligned} A &= -\frac{r}{J\bar{v}} \begin{bmatrix} \delta\bar{\Psi}_{f,f} & \delta\bar{\Psi}_{f,r} \\ \delta\bar{\Psi}_{r,f} & \delta\bar{\Psi}_{r,r} \end{bmatrix}, \\ B &= \frac{r}{J\bar{v}} \begin{bmatrix} 1 & 0 \\ 0 & 1 \end{bmatrix}, \\ C &= \begin{bmatrix} 1 & 0 \\ 0 & 1 \end{bmatrix}. \end{aligned}$$

Thus, computing  $G(s) = C(sI - A)^{-1}B$ , yields

$$G(s) = \frac{r/J\bar{v}}{D(s)} \begin{bmatrix} (s + \frac{r}{J\bar{v}}\delta\bar{\Psi}_{r,r}) & -\frac{r}{J\bar{v}}\delta\bar{\Psi}_{f,r} \\ -\frac{r}{J\bar{v}}\delta\bar{\Psi}_{r,f} & (s + \frac{r}{J\bar{v}}\delta\bar{\Psi}_{f,f}) \end{bmatrix}, \quad (2.70)$$

with

$$D(s) = s^2 + \frac{r}{J\bar{v}}(\delta\bar{\Psi}_{f,f} + \delta\bar{\Psi}_{r,r})s + \left[\frac{r}{J\bar{v}}\right]^2 (\delta\bar{\Psi}_{f,f}\delta\bar{\Psi}_{r,r} - \delta\bar{\Psi}_{f,r}\delta\bar{\Psi}_{r,f}). \quad (2.71)$$

### 2.5.2.3 Stability Analysis

Based on the transfer function matrix (2.70), the stability and minimum-phase properties of the linearised double-corner model can be easily analysed.

The linearised double-corner model with transfer function matrix (2.70) is asymptotically stable if and only if the coefficients of the denominator  $D(s)$  in (2.71) are non-zero and have the same sign<sup>4</sup>.

To work out this condition in a meaningful and readable manner, we proceed by assuming that the front wheel dynamics are independent of those of the rear wheel, *i.e.*, we disregard the dependence of  $\Psi_f(\lambda_f, \lambda_r)$  from  $\lambda_r$  and set  $\delta\bar{\Psi}_{f,r} = 0$ . This assumption is motivated by the analysis carried out in

---

<sup>4</sup> For a second-order polynomial, this is a necessary and sufficient condition for its roots to have negative real part.

Section 2.4 (see also Figures 2.12(a) and 2.12(b)). Further, we perform the linearisation about  $\bar{\lambda}_f = \bar{\lambda}_r = \bar{\lambda}$ .

Under this assumption, one has asymptotic stability of the linearised model if and only if

$$\begin{cases} \delta\bar{\Psi}_{f,f} + \delta\bar{\Psi}_{r,r} > 0, \\ \delta\bar{\Psi}_{f,f}\delta\bar{\Psi}_{r,r} > 0. \end{cases} \quad (2.72)$$

In view of the above assumptions and of the expressions of  $\delta\bar{\Psi}_{f,f}$  and  $\delta\bar{\Psi}_{r,r}$  in (2.61) and (2.64), the first equation of (2.72) has the form

$$\begin{aligned} \delta\bar{\Psi}_{f,f} + \delta\bar{\Psi}_{r,r} &= r(W_f + W_r)\mu_1(\bar{\lambda}) - 2\frac{J}{r}\bar{v}_+ \\ &+ \frac{J}{r}(1 - \bar{\lambda})[\bar{v}_{+,f} + \bar{v}_{+,r}] + r\Delta_{F_z}\mu(\bar{\lambda})[\bar{v}_{+,f} - \bar{v}_{+,r}] \\ &= r(W_f + W_r)\mu_1(\bar{\lambda}) \left[ 1 + \frac{J}{r^2M} \left( -2\frac{\mu(\bar{\lambda})}{\mu_1(\bar{\lambda})} + (1 - \bar{\lambda}) \right) + \frac{2\Delta_{F_z}\mu(\bar{\lambda})^2}{M^2} \right] > 0, \end{aligned}$$

which, considering that  $J/(r^2M) \ll 1$  reduces to  $\mu_1(\bar{\lambda}) > 0$ .

Analysing now the second condition (2.72), one obtains

$$\begin{aligned} \delta\bar{\Psi}_{f,f}\delta\bar{\Psi}_{r,r} &= r^2W_fW_r\mu_1(\bar{\lambda})^2 + \left( \frac{J^2}{r^2} - r^2\Delta_{F_z}^2\mu_1(\bar{\lambda})^2 \right) \bar{v}_+^2 \\ &+ \left( \frac{J^2}{r^2}(1 - \bar{\lambda})^2 - r^2\Delta_{F_z}^2\mu(\bar{\lambda})^2 \right) [\bar{v}_{+,f}\bar{v}_{+,r}] \\ &\cong r^2W_fW_r\mu_1(\bar{\lambda})^2 \left[ 1 - \frac{\Delta_{F_z}^2\mu(\bar{\lambda})^2}{M^2} \frac{(W_f + W_r)^2}{W_fW_r} - \frac{\Delta_{F_z}^2\mu(\bar{\lambda})^2}{M^2} \right] > 0, \end{aligned}$$

which, considering that the two negative terms in the square brackets are both  $\ll 1$ , is trivially satisfied for all choices of the linearisation point.

This analysis shows that the linearised system with transfer function  $G(s)$  is open-loop unstable if the equilibrium  $(\bar{\lambda}_f, \bar{\lambda}_r)$  occurs beyond the peak of the curve  $\mu(\lambda)$ , thus yielding the same stability condition found for the single-corner model.

Further, it is interesting to note that the static gain of  $G_{ff}(s)$  is given by

$$G_{ff}(0) = \frac{\delta\bar{\Psi}_{r,r}}{(\delta\bar{\Psi}_{f,f}\delta\bar{\Psi}_{r,r} - \delta\bar{\Psi}_{f,r}\delta\bar{\Psi}_{r,f})} \cong \frac{1}{\delta\bar{\Psi}_{f,f}}, \quad (2.73)$$

while similarly that of  $G_{rr}(s)$  has the form

$$G_{rr}(0) = \frac{\delta\bar{\Psi}_{f,f}}{(\delta\bar{\Psi}_{f,f}\delta\bar{\Psi}_{r,r} - \delta\bar{\Psi}_{f,r}\delta\bar{\Psi}_{r,f})} \cong \frac{1}{\delta\bar{\Psi}_{r,r}}. \quad (2.74)$$

By analysing the expression of  $\delta\bar{\Psi}_{f,f}$  in (2.61) and observing that  $\bar{v}_{+,r} > 0$  if and only if  $\mu_1(\bar{\lambda}) > 0$  (see Equation 2.66), one has that the static gain of  $G_{ff}(s)$  is positive if the linearisation point is before the peak of the friction curve (note that the same was true for the single-corner model, see Equation 2.54). To see that this holds also for  $G_{rr}(s)$ , consider the expression of  $\delta\bar{\Psi}_{r,r}$  in (2.64), which can be rewritten as

$$\begin{aligned}\delta\bar{\Psi}_{r,r} &= rW_r\mu_1(\bar{\lambda}) - \frac{rW_r\Delta_{F_z}\mu(\bar{\lambda})\mu_1(\bar{\lambda})}{M} \\ &\quad - \frac{r(W_f + W_r)\Delta_{F_z}\mu(\bar{\lambda})\mu_1(\bar{\lambda})}{M} \left[ 1 + \frac{\Delta_{F_z}\mu(\bar{\lambda})}{M} \right] \\ &\cong rW_r\mu_1(\bar{\lambda}) \left[ 1 - \frac{\Delta_{F_z}\mu(\bar{\lambda})}{M} \left( 1 + \frac{(W_f + W_r)}{W_r} \right) \right] \cong rW_r\mu_1(\bar{\lambda}).\end{aligned}$$

Finally, the zero of the transfer functions  $G_{ff}(s)$  and  $G_{rr}(s)$  has the form

$$s_z = -\frac{r}{J\bar{v}}\delta\bar{\Psi}_{i,i}, \quad i = \{f, r\}.$$

Thus, the zero is negative if and only if  $\delta\bar{\Psi}_{i,i} > 0$  and this, as shown above, happens when  $\mu_1(\bar{\lambda}) > 0$ , thus again yielding results that are qualitatively equal to those obtained for the single-corner model.

Moving to the transfer functions  $G_{ij}(s)$ ,  $i = \{f, r\}$  of the coupling terms, one has that the static gain is given by

$$G_{ij}(0) = \frac{-\delta\bar{\Psi}_{i,j}}{\frac{r}{J\bar{v}}(\delta\bar{\Psi}_{i,i}\delta\bar{\Psi}_{j,j} - \delta\bar{\Psi}_{i,j}\delta\bar{\Psi}_{j,i})} \cong \frac{-\delta\bar{\Psi}_{i,j}}{\frac{r}{J\bar{v}}(\delta\bar{\Psi}_{i,i}\delta\bar{\Psi}_{j,j})}. \quad (2.75)$$

Thus, while the static gain of the direct transfer functions  $G_{ff}(s)$  and  $G_{rr}(s)$  is independent of  $\bar{v}$  as it was for the single-corner model, see Equation 2.54, this is not true for the transfer functions of the coupling terms, whose static gain is inversely proportional to  $\bar{v}$ . Further, note that the static gain of the transfer function  $G_{rf}(s)$  is positive for all linearisation points with  $\mu_1(\bar{\lambda}) > 0$ , as – see Equation 2.63 – one has that

$$\delta\bar{\Psi}_{r,f} \cong -r\Delta_{F_z}\mu(\bar{\lambda})\mu_1(\bar{\lambda})\frac{W_f}{m}. \quad (2.76)$$

Conversely, the static gain of the transfer function  $G_{fr}(s)$  is negative for all linearisation points with  $\mu_1(\bar{\lambda}) > 0$ , as – see Equation 2.62 – one has that

$$\delta\bar{\Psi}_{f,r} \cong r\Delta_{F_z}\mu(\bar{\lambda})\mu_1(\bar{\lambda})\frac{W_r}{m}. \quad (2.77)$$

Finally, the high frequency gain for the direct terms  $G_{ff}(s)$  and  $G_{rr}(s)$  has the form



$$\lim_{s \rightarrow \infty} s G_{ii}(s) = \frac{r}{J\bar{v}}, \quad i = \{f, r\}, \quad (2.78)$$

as was the case for the single-corner model, see Equation 2.55, while for the coupling terms it is given by

$$\lim_{s \rightarrow \infty} s^2 G_{ij}(s) = - \left[ \frac{r}{J\bar{v}} \right]^2 \delta \bar{\Psi}_{i,j}, \quad i = \{f, r\}. \quad (2.79)$$

**Table 2.5** Nominal linearisation conditions for the double-corner model

Variable	Steady-state value
$\bar{\lambda}_f$	0.05
$\bar{\lambda}_r$	0.07
$\bar{T}_{bf}$	859 Nm
$\bar{T}_{br}$	395 Nm
$\bar{v}$	25 m/s
$\ddot{v}$	-8.8 m/s <sup>2</sup>
$F_{zf}$	3.193.2 N
$F_{zr}$	1221.5 N
Road conditions	Dry asphalt (see Table 2.1)

### 2.5.2.4 Numerical Sensitivity Analysis

For the double-corner model, the analysis is carried out for the equilibrium point characterised by the values given in Table 2.5, which reports the linearisation conditions for the double-corner model. To analyse the open-loop behaviour of the transfer function matrix (2.68), let us refer to Figures 2.13 and 2.14, where the magnitude and phase Bode plots of frequency responses associated with the transfer functions in (2.68) are plotted. Note further that to perform a comparison with the single-corner model, the transfer functions  $G_{ff}(s)$  and  $G_{rr}(s)$  are also compared with their single-corner counterparts. The latter have been obtained employing the steady-state values in Table 2.5.

- **Single-corner *versus* Double-corner Model**

The comparison is done first of all by analysing the transfer functions  $G_{ff}(s)$  and  $G_{rr}(s)$  and their counterparts obtained with the single-corner model. As can be seen, the single-corner model and the double-corner model do not show significant differences. This is due to the fact that considering Equation 2.71 and assuming again to disregard the dependency of  $\Psi_f(\lambda_f, \lambda_r)$  from  $\lambda_r$ , *i.e.*, setting  $\delta \bar{\Psi}_{f,r} = 0$ , one has that the denominator  $D(s)$  in (2.71) takes the form

$$D(s) = \left( s + \frac{r}{J\bar{v}} \delta \bar{\Psi}_{f,f} \right) \left( s + \frac{r}{J\bar{v}} \delta \bar{\Psi}_{r,r} \right). \quad (2.80)$$

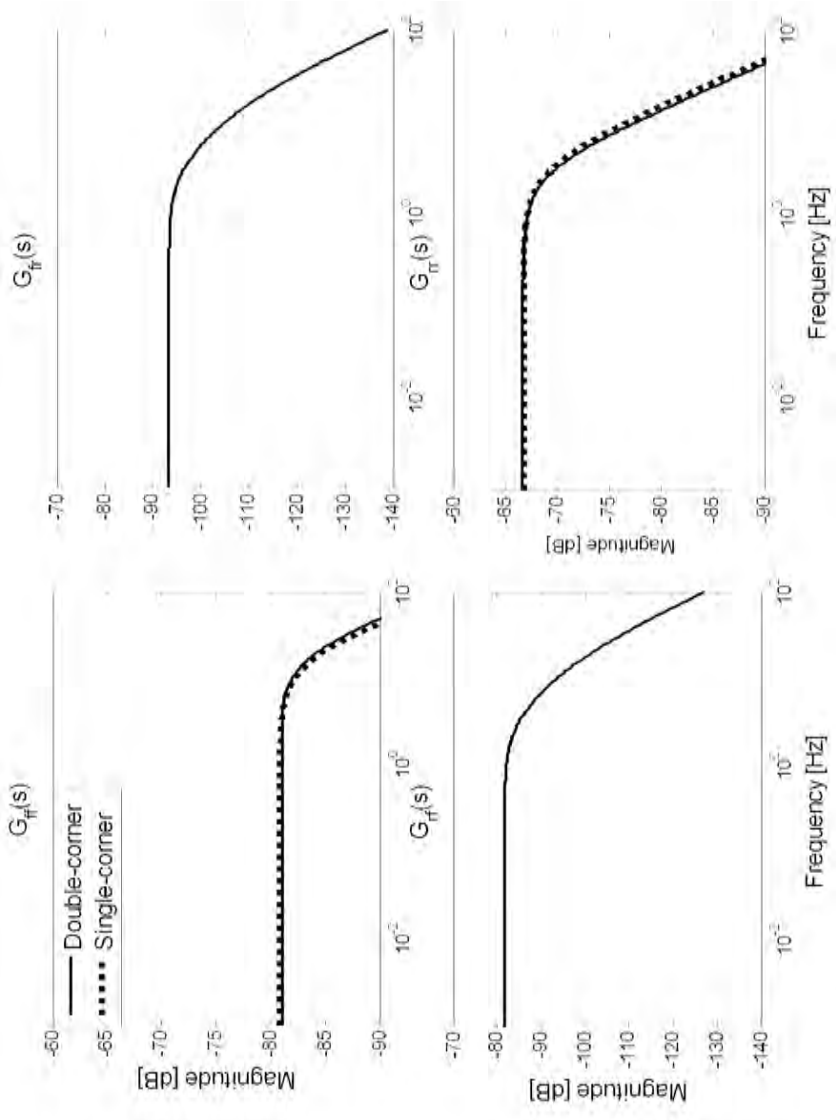


**Figure 2.13** Magnitude Bode plots of the frequency response associated with the transfer function matrix (2.68)

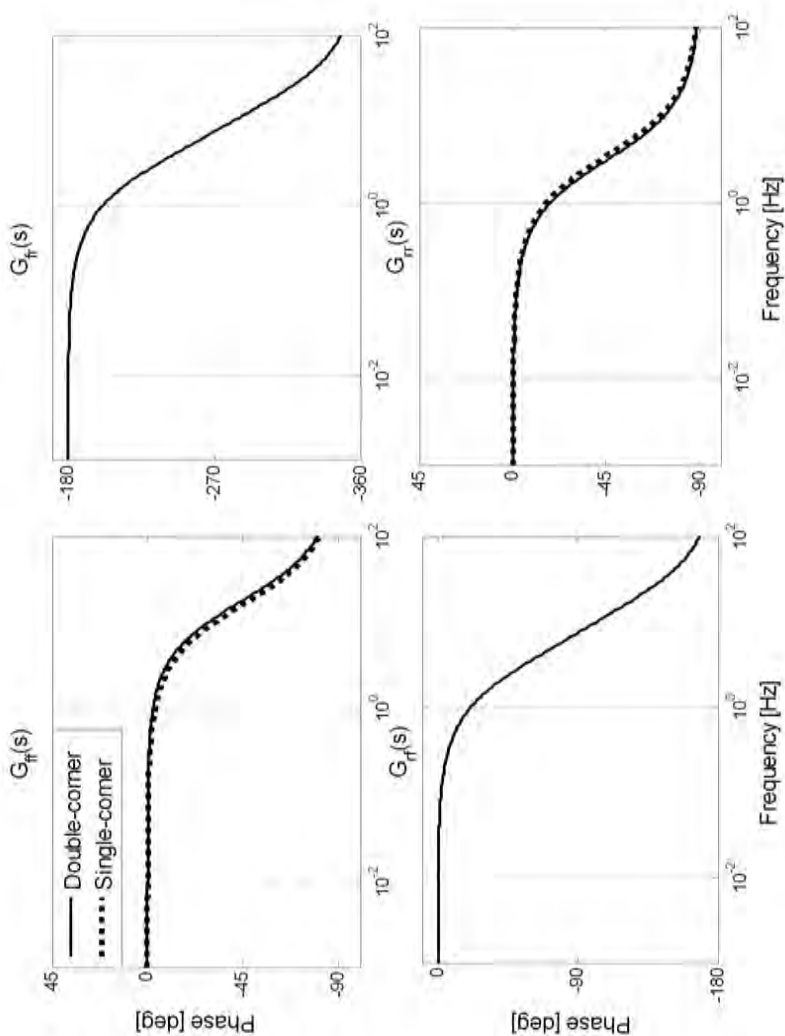


**Figure 2.14** Phase Bode plots of the frequency response associated with the transfer function matrix (2.68)

Thus, under this assumption there is a cancellation between one of the poles and the zero of the direct terms, see Equation 2.70, and the double-corner model reduces in fact to the single-corner one. Actually, if no assumptions are made, the cancellation is not exact but nonetheless tends to cancel out the effects of the pole and of the zero, which indeed remain quite close. Further, coherently with the analysis carried out on the high-frequency gain, the single-corner and the double-corner model share the

same behaviour at high frequency. Due to this fact, the effects of longitudinal vehicle speed variations act as a frequency scaling on the transfer functions  $G_{ff}(s)$  and  $G_{rr}(s)$  of the double-corner model exactly in the same way as they do for the single-corner model, see Equations 2.55 and 2.78.

### • Coupling Terms

The most interesting feature of the double-corner model is its ability to describe the dynamic coupling between front and rear axles. As can be seen from Figure 2.13 the static gain of the coupling terms  $G_{fr}(s)$  and  $G_{rf}(s)$  is of the same magnitude as that of the *direct* transfer functions  $G_{ff}(s)$  and  $G_{rr}(s)$ .

Finally, the phase diagram in Figure 2.14 allows us to confirm the behaviour of the static gains of the coupling terms outlined in Equations 2.76 and 2.77. Specifically, the cross coupling term  $G_{rf}(s)$  has negative static gain. This has the following intuitive physical interpretation: when a constant braking torque is applied to the front wheel, the front wheel slip  $\lambda_f$  increases (recall that  $\lambda$  is positive during braking) and this in turn causes the vehicle speed  $v$  to decrease. Hence, the effect on the rear axle (whose wheel speed  $\omega_r$  is unaffected by the change on  $\lambda_f$ ) is a decrease in the rear wheel slip as  $\lambda_r = 1 - r\omega_r/v$ . Note that this is in principle true also for the effect of the rear wheel on the front one, but because the effect of the rear wheel slip on the front one is very weak this is not evident.

## 2.6 Summary

In this chapter the adopted analytical description of the tyre-road contact forces was introduced and the dynamical models of the braking dynamics, which will serve as a basis in the control design phase, namely the single-corner and the double-corner models, were described.

Specifically, a complete analysis was carried out, both on the nonlinear models and on their linearised versions, so as to highlight the equilibrium points, their stability properties as a function of the model parameters and the frequency response characteristics.

These results constitute the necessary background on braking dynamics analysis and will serve as a basis for the next chapters where active braking controllers will be designed.



<http://www.springer.com/978-1-84996-349-7>

Active Braking Control Systems Design for Vehicles

Savaresi, S.M.; Tanelli, M.

2010, XXI, 254 p., Hardcover

ISBN: 978-1-84996-349-7